Chapter 1
Nanotechnology in Mechanobiology: Mechanical Manipulation of Cells and Organelle While Monitoring Intracellular Signaling

Hitoshi Tatsumi, Kimihide Hayakawa, and Masahiro Sokabe

1.1 Introduction

Cell migration requires a regulated interplay of actin-filament dynamics and turnover of cell-matrix adhesions (Pollard and Borisy 2003; Ridley et al. 2003). These processes are mechanically coupled by a large complex of cytoplasmic proteins linking adhesive molecules to cytoskeletons (Zamir et al. 1999; Szaszak et al. 2002). The response of vascular endothelial cells to cyclic stretching is an excellent example of mechano-induced morphological change. Endothelial cells in vivo show a spindle-like shape aligning their long axis parallel to the vessel running. When the cells are cultured on an elastic sheet, they show a polygonal shape with random orientation. However, when they are subjected to uni-axial cyclic stretch, they start to change their shape from a cobble-like shape to a spindle-like shape, aligning their long axis perpendicular to the stretch axis (Shirinsky et al. 1989; Naruse et al. 1998b) as seen in the vessel wall in vivo. Focal contacts (FCs) and cytoskeletons play crucial roles to maintain the shape of the endothelial cells (Drake et al. 1992; Kawakami et al. 2001). Redistributions of FCs and cytoskeletons are necessary for the shape remodeling of cells. Mechanosensing machinery followed by intracellular signaling and redistribution of FCs must be elucidated to understand the molecular process underlying the shape remodeling of the cell in response to mechanical stimuli. To explore the molecular mechanisms underlying the force-dependent cell shape remodeling, it is crucial to apply precisely controlled mechanical stimuli (ranging from pN to nN) to FCs and to observe the response with a high spatial–temporal resolution (ranging from 100 nm to 1 μm, and 1 ms to 1 min) in living cells. In this chapter, we

H. Tatsumi (✉) and M. Sokabe
Department of Physiology, Nagoya University Graduate School of Medicine,
65 Tsurumai, Showa-ku, Nagoya, Aichi 466-8550, Japan
e-mail: tatsumi@med.nagoya-u.ac.jp

K. Hayakawa and M. Sokabe
ICORP/ORST, Cell Mechanosensing Project, Japan Science and Technology Agency,
Nagoya, Aichi 466-8550, Japan

M. Noda (ed.), *Mechanosensing Biology*,
DOI 10.1007/978-4-431-89757-6_1, © Springer 2011

describe a variety of methods for controlled mechanical stimulations as well as the laboratory systems for monitoring the mechanosensing, and the mechano-induced signaling, e.g., activation of mechanosensitive (MS) channels, intracellular calcium ion concentration ($[Ca^{2+}]_i$) increases, adhesive contact formation and mechano-induced reorganization of cytoskeletons in live cells including neuronal growth cones and human umbilical vein endothelial cells (HUVECs).

1.2 A Variety of Methods for Applying Forces to Cells and Analyses of Mechanosensing and Signaling

1.2.1 Stretching Cells Cultured on Elastic Sheets

Two types of methods for stretching cells on an elastic sheets have been reported; one is a flexible (elastic)-bottomed cultured plate (Fig. 1.1a) (Iba and Sumpio 1991) and the other is a square elastic sheet for uni-axial stretching (Naruse et al. 1998b) (Fig. 1.1c). Cells are cultured on an elastic sheet coated with extracellular matrix like fibronectin, laminin or collagen, and subjected to stretch. In the first type, negative pressure (e.g., 150 mmHg pressure) is applied to the elastic plate to expand the cell substratum, and cells are stretched. The experimental setup is simple, and the amplitude and duration of stretching are controlled by changing the amplitude and duration of applied negative pressure. It should be noted that the direction and amplitude of stretching are dependent on the place of a cell in the plate; e.g., cells in the center of a plate are stretched in all directions, while the cells near 12 o'clock are stretched in the 6–12 o'clock direction (see Fig. 1.1b). The amplitude of stretching is also dependent on the place of a cell in the plate; the largest stretching (e.g., 24%) is applied to the cells in the periphery and it declines as cells are located towards the center of the plate (e.g., 1%) (Iba and Sumpio 1991). A merit of this technique is that we can immediately get a variety of responses depending on the place of the cells if we correctly distinguish the differences. At the same time, however, this merit turns out to be a demerit when we make a biochemical mass analysis, since the cells in a dish give an average of mixed responses.

A square elastic sheet is used for uni-axial stretching. The machinery as shown in Fig. 1.1c stretches the chamber. Cells are stretched in the same direction, and most of the cells are stretched in the same amplitude; however, slightly less stretching is applied to the cells at the margin of the chamber. With this type of machinery, FCs aligning their long axis parallel to the stretch axis disappear and those perpendicular to the stretch axis elongate during the cyclic stretching (Naruse et al. 1998a). Cells can be observed before and after cyclic stretching with an objective lens, as shown in the Fig. 1.1d, which also enables monitoring the response, e.g., intracellular Ca ion concentration ($[Ca^{2+}]_i$) changes. These methods enable slow and creeping analyses of mechanical stimuli-dependent cell-remodeling, and the biochemical process behind it (see more details in Shi et al. 2007; Wang et al. 2001).

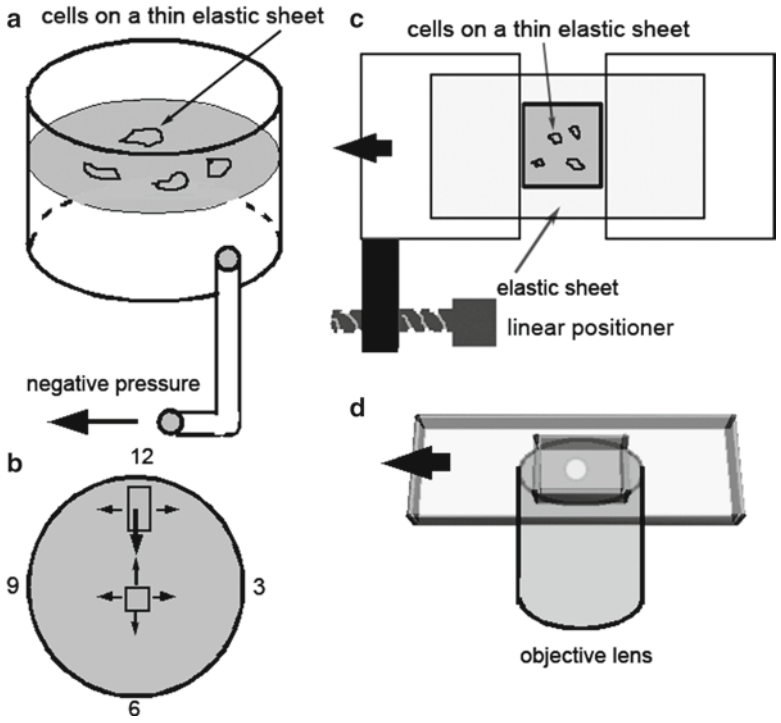

Fig. 1.1 Methods for stretching cells cultured on an elastic sheet. A flexible (elastic)-bottomed culture sheet (**a**) and an elastic sheet for uni-axial stretching (**c**) are shown schematically. Cells are cultured on elastic sheets and subjected to stretch. (**a**) Negative pressure is applied to the elastic plate to expand the cell substratum. Cells in the center of the plate are stretched in all directions, while the cells, e.g., in the 12 o'clock are stretched in the 6–12 o'clock direction (**b**). The *arrows* show the direction and amplitude of the stretching. (**c**) A square elastic sheet is used for uni-axial stretching. Cells are cultured on a square chamber slide with a thin elastic substratum. A thick elastic sheet is attached on the rigid materials; the *left side* of the elastic sheet is stretched with a linear positioner driven by a stepping motor. Elastic plates and cells are placed above an objective lens (**d**). These stretching systems are commercially available from Flexcell Corp. (http://www.flexcellint.com/) and Scholertec (http://www2.odn.ne.jp/stec/)

1.2.2 Localized Force Application by Dragging a Pipette While Recording Intracellular Signaling

Force can be applied to a cell by dragging a pipette as shown in Fig. 1.2a. The highly precise mechanical stimulus can be applied to different parts of dorsal root ganglion (DRG) neurons, using a piezo-driven glass microcapillary whose movement is computer-controlled (Imai et al. 2000). The DRG neurons are primary afferent neurons, which carry sensory signals from the skin of the limbs and the trunk, muscle and visceral organs to the spinal cord. Various mechanical, thermal, chemical, and/or noxious events are known to generate action potentials at the peripheral nerve

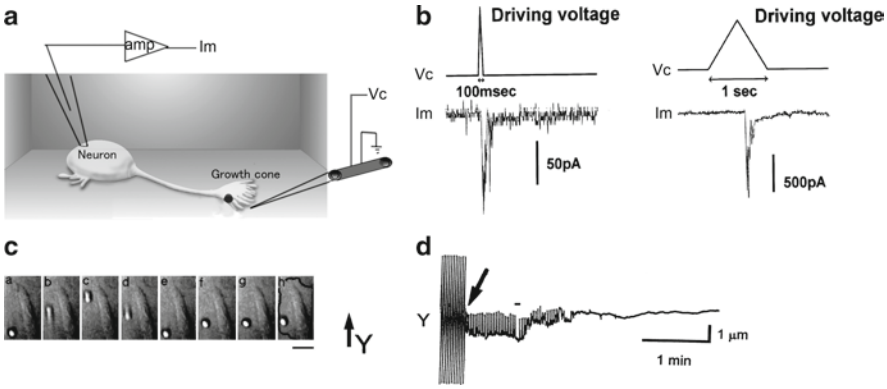

Fig. 1.2 Schematic drawing of a piezo-driven pipette and optical trapping of a bead for applying force and analyzing the mechano-induced response in growth cones. (**a**) A neuron with a growth cone and a piezo-driven pipette. (**b**) Driving voltage (triangular pulses) of various durations (100 ms and 1 s) was applied to piezo-actuators to make horizontal movements of the tip of a glass microcapillary. After the tip reached its maximal displacement at the top of the triangular pulse, the tip returned to the initial position. The control signal is shown (Vc). The inward current induced by the mechanical stimuli is shown in trace (Im). The current was evoked near the maximum displacement of the tip. (**c**) A polarized beam from a laser was focused on a bead on a growth cone to trap and drag the bead in Y direction. The bead stays on the growth cone (f, g, h panels) after electrical stimulation. *Horizontal bar* denotes 2 μm. (**d**) Analysis of optical tweezers-induced movement of beads before and after the adhesion on the growth cone membrane. The bead attached on the growth cone and was slightly displaced along the *Y*-axis by optical trapping (*arrows*). The maximum distance of bead movement by the optical trapping decreased and finally became almost zero after 10 min of observation, indicating that optical trapping could no longer move the beads. Some of the data are based on our previous reports (Tatsumi and Katayama 1999; Imai et al. 2000); they are modified and presented in panels (**b**)–(**d**)

endings of DRG neurons. It is plausible that the peripheral nerve endings of DRG neurons possess a variety of membrane sensory receptors activated by mechanical, thermal, chemical, or noxious stimuli. There is a wide consensus that the membrane of growth cones formed at the nerve endings undergoes large changes in tension during extension and retraction of neurites. It is assumed that these regions are endowed with MS machinery such as stretch-activated channels. However, the mechanism of mechanoelectric transduction at the peripheral nerve endings of DRG neurons is poorly understood. We examined the whole cell current induced by mechanical stimulation, and explored the distribution of sensing machinery.

The schematic drawing in Fig. 1.2 shows the design of the pipette attached to the piezo-actuator and the voltage signal for controlling the piezo-actuator. A driving voltage (triangular pulses) of various amplitudes and durations (100 ms to 1 s) was applied to the piezo actuators to make horizontal movement of the tip of the glass microcapillary in the order of 0–3.9 μm. The tip reached its maximal displacement at the top of the triangular pulse, and subsequently the tip returned to the initial position. The mechanical stimulation induced an inward Cl^- current (Im) in the case of DRG growth cones, as shown in Fig. 1.2. Detailed analyses of the current can be

found in our report (Imai et al. 2000). The tips used for mechanical stimulation are heat-polished and rounded with tip diameters of 1–2 μm. The image of the experiment and the control signal are shown in Fig. 1.2. Filopodia as well as lamellipodia of growth cones were most sensitive to mechanical stimuli. However, when the neurite or soma of DRG cells was stimulated in the same way, electrical responses were hardly recorded, suggesting that the MS Cl^- channels were not distributed uniformly in dorsal root neurons. More detailed analyses of the current are reported elsewhere (Imai et al. 2000).

Force application by dragging pipette is also used to examine the role of tension in the formation of actin filament bundles (Hirata et al. 2004). A bent glass micropipette coated with glutaraldehyde was attached horizontally on an intact lamella of a semi-intact cell and displaced in parallel to the cell's longitudinal axis. The traction force causes formation of actin bundles parallel to the force direction. The micropipette was treated with 3-aminopropyltriethoxysilane, dried, coated with 20% glutaraldehyde for 5 min at room temperature, and washed before use, which makes a tight contact between the pipette and the cell surface. The horizontally placed outer wall of the bent tip of the micropipette was attached on the surface lamella of a semi-intact cell, and then the lamella could be dragged as the pipette moved horizontally.

1.2.3 Mechanical Force Application to the Cell Surface by Optically Dragging a Bead for Analyzing the Contact Formation

Optical trapping and dragging a bead can be used for applying forces to the cell (Dai and Sheetz 1995, 1999; Tatsumi and Katayama 1999; Giannone et al. 2003). These studies applied forces to the beads to measure the properties of the cell membrane or adhesive structures.

Growth cone migration depends on interactions between cell-surface adhesion receptors and components of the extracellular matrix. It has also been suggested that cell migration results from the generation of traction forces generated in the cytoskeleton at the sites of cell adhesion (Dembo and Wang 1999). The neuronal growth cone is important for axonal guidance and elongation. Contact between a growth cone and the target cell initiates synapse formation, and the importance of cell–cell adhesive molecules for path finding and synapse formation has also been suggested. However, cell–cell adhesive contacts at the growth cone of living neurons have been observed in only a few studies. Activity-dependent transmitter release and adhesive cell–cell interactions have been studied separately; however, the relationship between these events has been examined in mammalian central neurons by us (Tatsumi and Katayama 1999). The properties of the adhesive contact at the growth cones of the diagonal band of Broca (DBB), a well-known cholinergic center in the mammalian brain, were studied by optically manipulating a latex bead attached to the growth cone surface. To examine the cellular response just after the formation of adhesive contact, small beads which were optically trapped were

repeatedly attached to and detached from the growth cone membrane (Fig. 1.2c). While this procedure of attachment and detachment was repeated, electrical stimulation was applied to the DBB cell body. The bead attached to and stayed on the growth cone within 2 min of the stimulation due to the contact formation.

This maintained contact was observed in 40% of beads examined. The optical force moved the bead to the limit of dragging because of the contact formation, and the bead was released from the optical trap (see Fig. 1.2d), suggesting that a submembrane barrier (e.g., cytoskeletons) disturbs the dragging of the bead by the trapping force as reported previously. Then, the bead returned to the original position (or attached point). In all cases, the movable distance (denoted in Fig. 1.2d by an arrow) of the bead by the laser force gradually decreased, and finally the optical force did not move beads after 10 min of observation, suggesting that surface structures bound to the bead began to be associated with rigid cytoskeletal structures. Recent progress using knockout cell lines shows that talin1 is involved in the force-dependent reinforcement of initial integrin–cytoskeleton bonds in human melanoma lines (Giannone et al. 2003).

Optical trapping and dragging of a bead (shown in Fig. 1.2c) were made as follows (see also Fig. 1.5a): a polarized beam from a 50-mW red (643 nm) Argon–Krypton laser (model 643-100RS; Omnichrome, CA) or 250 mW near-infrared (1,064 nm) YAG laser (model DPY321; Coherent, CA) was focused through a water-immersion objective lens (×63, NA 1.2; Zeiss, Germany; or ×100 NA 1.45; Nikon, Japan) on a small Latex bead (0.52 μm diameter, carboxylate microspheres; Polysciences, PA) on the growth cone (Fig. 1.2a). A remote mirror steering system (Nanomover; Melles Griot, Japan) was placed to steer the laser trapping point. The maximum particle retention force of the laser optical trapping was 0.7 pN in our setup (Block 1990). Latex beads were treated with bovine serum albumin (5 mg/ml) and were applied to growth cones. These beads have also been used as cell surface markers in experiments using molluscan neuronal growth cones. A single bead was trapped and slowly displaced by moving the trapping point on the lamellipodium of the growth cone.

1.2.4 Force Application Via a Bead Attached on the Surface of a Cell for the Analyses with High Spatial–Temporal Resolution

High-speed, single-cell analyses at the molecular level are crucial to elucidate the mechanism underlying the mechanosensing and mechano-induced remodeling of cells. However, detailed analyses could not be made during cyclic stretching of the cell substrate, since cells escape from the view of the microscope during the stretching (Fig. 1.1d). We have developed a new assay system to apply localized mechanical stress to an endothelial cell by using a fibronectin-conjugated bead (FN-bead), which enables imaging of individual FCs during the mechanical stimulation and recording mechano-induced responses. The values mentioned in this section are used to analyze and explore the molecular mechanism underlying the

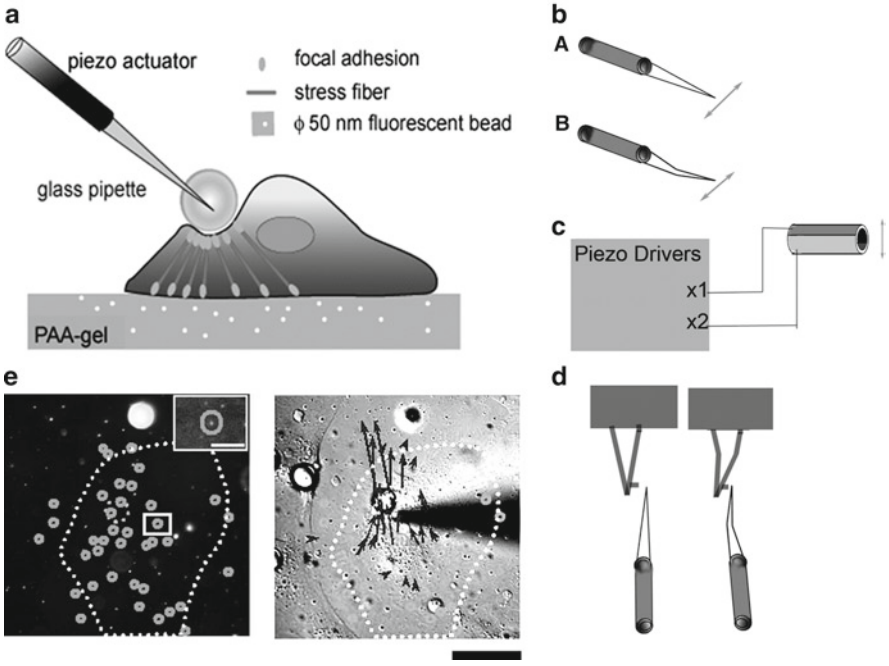

Fig. 1.3 Mechanical stimulation by displacing a FN-bead. (**a**) Schematic drawing of a bead on a cell. A FN-coated bead was displaced by a piezo-driven glass pipette, which gives localized mechanical force to the cell surface and the FCs. A glass micropipette is attached at the tip of a piezo-actuator as shown in (**b**); straight type (**A**) and bent type (**B**). The bent type was suitable for a displacement in parallel to the cell substratum. (**c**) The amplitude of the force applied to the bead is controlled with piezo-drivers (Actuator driver, ENP-5041BS; ECHO Electronics). The output X1 and X2 are applied to the half of cylindrical piezo actuators (Fuji Ceramics, Tokyo Japan), respectively, in the anti-phase; e.g., one +50 V and the other −50 V from a basal bias voltage of 100 V. (**d**) Stiffness of the tip of the glass capillary is estimated by bending the tip of an AFM probe (SN-AF01; Olympus, Japan). (**e**) An example of gel deformation caused by the mechanical stimulation. An FN-bead (shown by a *circle* in the DIC image in the *right*) on a HUVEC (denoted by the *white broken line* that denotes the cell perimeter) was displaced by a piezoelectric-driven glass pipette (a *shadow* in the DIC image). *Small gray circles* indicate the position of 50 nm fluorescent beads (*left panel*). Insets show fluorescent beads at higher magnification (a fluorescent spot at the center of the circle; *scale bar*, 20 μm). Each *arrow* in the *bottom panel* indicates the direction and relative amplitude of fluorescent particle displacement (*longest arrow* corresponds to 0.76 μm displacement) when the FN-bead was moved 4 μm in the direction shown by *arrows*. Data in panel (**e**) are based on our previous report (Hayakawa et al. 2008)

mechano-induced channel activation and intracellular calcium ion concentration increases (see Sects. 1.2.6 and 1.2.7).

FN-beads are plated on HUVECs (Fig. 1.3a). The FN-beads adhere to the cell surface within a few minutes after their plating as in the case of growth cones (Fig. 1.2). Integrin, paxillin, and vinculin were accumulated beneath the beads within 5 min, showing that FCs were formed beneath the beads (Hayakawa et al. 2008). These FCs are generally connected to the basal FCs via actin stress fibers

within 30 min. Glass beads (Φ 10 μm; Duke Scientific, USA) are conjugated with fibronectin as described previously (Jacobson et al. 1978).

By displacing a bead with a glass capillary localized mechanical force was applied to the basal FCs via actin stress fibers that connect the FCs beneath the bead and the FCs at the bottom of the cell, as schematically drawn in Fig. 1.3a. A FN-coated bead can be displaced precisely by a piezo-driven glass pipette (approximately 1 μm) for 100 ms. The force required to displace the FN bead for 1 μm was estimated at approximately 30 nN using a calibrated micropipette in our experimental setup (10 μm bead on endothelial cells). The pipette was made from glass capillary (1 mm; Narishige, Japan) with a programmable puller (Model P-97; Sutter Instruments, USA) that could reproduce pipettes with almost the same shaped tip under controlled temperature environments. The stiffness of the tip of the glass capillary was estimated by bending the tip using a calibrated tip of an AFM probe (SN-AF01; Olympus, Japan); the displacement of an FN-bead and bending of the tip of the capillary were monitored with a CCD camera to estimate the force. The force applied to the bead was estimated from the relation between the displacement of the FN-bead and the bending of the tip of the glass capillary (Fig. 1.3d). The force required for 1 μm displacement of the FN bead was estimated at 35.7 ± 5 nN ($n = 5$) in our conditions.

To elucidate the area where the force was transmitted by FN-bead displacement, we employed a polyacrylamide gel substrate culture system based on (Munevar et al. 2001). HUVECs are cultured on a fibronectin-conjugated polyacrylamide gel containing fluorescent particles (Φ 50 nm) for time-lapse imaging of the deformation of the gel (Fig. 1.3a). The time-dependent changes in the mechanical force generated by displacement of the FN bead can be examined by time-lapse recording of the fluorescent particles embedded in the substrate; translocation of beads reflects the deformation of the substrate. The amplitude and direction of deformation in the gel upon displacement of a FN bead by 4 μm were estimated (Fig. 1.3e). The image analysis of movements of the fluorescent particles showed that the mechanical force was transmitted to the area approximately 20 μm from the bead, where the substrate was moved in the direction of bead displacement.

Apical surface of the ells pretreated with cytochalasin D (cytoD) (100 nM, 30 min) could be deformed with a similar degree to that of the control FN-bead displacement, but the force required for the same displacement of the bead on the cytoD-treated cells was estimated at only 2.3 ± 0.5 nN ($n = 6$). This small amount is probably due to the disassembly of mechanically resistive stress fibers by cytoD, implying that the mechanical force was transmitted to the cell bottom via actin stress fibers.

1.2.5 Mechanical Stretching of Actin Stress Fibers by Displacing a FN-Bead to Activate MS Channels in HUVECs

To date, two mechanisms have been proposed for MS channel activation. One is that tension development in the lipid bilayer directly activates MS channels.

This is mostly based on biophysical analyses of the bacterial large conductance MS channel, MscL (Sukharev et al. 1999), and TRPC1 (Maroto et al. 2005) reconstituted in cytoskeleton-free liposomes. The second mechanism proposes that the extracellular matrix (Du et al. 1996) and cytoskeleton (Fukushige et al. 1999; Sokabe et al. 1991) are involved in channel activation; more specifically, tension in the cytoskeleton activates MS channels. A couple of studies (Byfield et al. 2004; Evans and Waugh 1977) have shown that a membrane interacting with cytoskeletons is stiffer than the membrane alone, implying that cytoskeletons would make the membrane a more efficient force-transmitting device. In fact, a certain MS channel shows a loss of mechanosensitivity in a cytoskeleton-free membrane (Zhang et al. 2000). It has also been reported that the cytoskeleton by itself will work as a force-focusing structure (Hu et al. 2003) owing to its linear structure with a relatively high elastic modulus (Kojima et al. 1994). Unfortunately, however, this idea is based on indirect evidence from electrophysiological and genetic analyses in eukaryotic cells (Corey et al. 2004). It is imperative to design and conduct experiments in which one can directly manipulate cytoskeletons while recording MS channel activities, preferably in intact cells.

We used intact cultured HUVECs to demonstrate that MS channels are activated by stress in the cytoskeleton. When HUVECs are subjected to uni-axial stretch, MS channels are activated, followed by an increase in the intracellular Ca^{2+} concentration ($[Ca^{2+}]_i$) because of Ca^{2+} influx through the channels (Naruse and Sokabe 1993). Stretching the extracellular substrate generates stress in the actin cytoskeleton (Pourati et al. 1998), which has been postulated to activate MS channels. However, detailed electrophysiological and imaging analyses of the channel activation is technically very difficult with this type of mechanical stimulation because of the movement of the cells upon stretching. We employed a new assay system that enables us to apply localized mechanical stresses onto focal adhesions to activate MS channels by dragging fibronectin-conjugated beads adhering to the dorsal cell surface or by injecting phalloidin-conjugated beads into cells (see Sect. 1.2.7), which then bind to actin stress fibers (and/or actin filaments). We demonstrated that direct mechanical stimulation (stretching) of the actin cytoskeleton using optical tweezers can activate MS channels in cultured HUVECs.

Immediately after a displacement of an FN bead, $[Ca^{2+}]_i$ increased rapidly and spread over the cell in a few seconds (Fig. 1.4c), then it returned to the resting $[Ca^{2+}]_i$ level in 3 min. The amplitude of the $[Ca^{2+}]_i$ increased monotonically with the degree of displacement (0.15–0.9 μm). The minimal response was induced by as short as 0.15 μm displacement (ca. 5.3 nN). The transient increase in $[Ca^{2+}]_i$ was largely inhibited (88.1 ± 4.3%, $n = 5$) by 20 μM Gd^{3+} or in Ca^{2+}-free medium, but was not affected by thapsigargin (1 μM), suggesting that the $[Ca^{2+}]_i$ increase was mediated by the influx of Ca^{2+} through MS channels.

We examined whether cytoskeletal structures were involved in the activation of the MS channels by FN-bead displacement. The FN-bead-dependent $[Ca^{2+}]_i$ increase was nearly perfectly abolished (95.1 ± 5.5%, $n = 3$) by the F-actin-disrupting agent cytoD (100 nM, 30 min). By contrast, the $[Ca^{2+}]_i$ increase was not affected by the microtubule-disrupting agent colcemid (1 μM, 30 min), suggesting that actin stress fibers are essential to induce the $[Ca^{2+}]_i$ increase by FN-bead displacement.

Electrophysiology should provide a better means than Ca^{2+} imaging to make quantitative analyses of the MS channel properties. For this purpose, we built a fully electronically controlled setup, shown in Fig. 1.4a, and made whole-cell patch-clamp recordings to monitor mechanically-induced channel currents. FN-bead

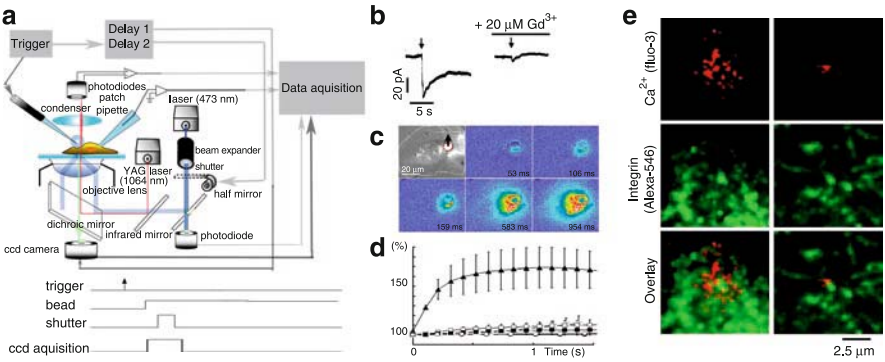

Fig. 1.4 High-speed imaging of $[Ca^{2+}]_i$ and the electrophysiological response induced by mechanical stimulation. (**a**) An electro-optical system for data acquisition. The trigger signal commands a piezo-driven glass pipette to move; the same signal triggers a focal plane shutter of a camera (α sweet; Minolta, Japan) after passing through a delay circuit. We put in a delay (e.g., 5 ms), since the piezo-driven glass pipette takes time to move. The signal also starts the acquisition of $[Ca^{2+}]_i$ images with a CCD camera under the control of software (MetaMorph; Universal Imaging, USA). The focal plane shutter enables brief (0.1 ms to 1 s) evanescent illumination of the specimen via a high NA (more than 1.4) lens; laser light is projected to the periphery of the objective lens to produce total internal reflection at the surface of the coverglass. We use evanescent (TIRF) illumination because it illuminates only the thin intracellular area near the bottom of the cell, which enables the recording of the rapid $[Ca^{2+}]_i$ increase beneath the membrane. To monitor the precise time of the illumination, half the laser power is projected to a photodiode. Signals of the bead movement, of laser illumination and of $[Ca^{2+}]_i$ image are fed into a data acquisition system. The time sequence of the trigger and the data acquisition is presented at *bottom* of the panel; trigger (an *arrow*), bead (bead movement detected with two photodiodes), shutter (laser illumination detected with diode) and CCD image acquisition. (**b**) Displacement of the bead induced an inward current. Gd^{3+} reduced the amplitude of the inward current. *Arrows* denote the displacement of the FN-bead. (**c**) Displacement of the FN-bead (1 μm for 100 ms) evoked an increase in $[Ca^{2+}]_i$. The *red circle* in the DIC image denotes the FN-bead. The *black arrow* indicates the direction of displacement. (**d**) $[Ca^{2+}]_i$ transients induced by bead displacement in different conditions. FN-bead displacement (1 μm for 100 ms) did not induce $[Ca^{2+}]_i$ increase in nominally Ca^{2+}-free solution (*asterisks*), and in solution contained 20 μM Gd^{3+} (*open squares*) or 100 nM cytochalasin D (*closed squares*). No $[Ca^{2+}]_i$ increase was also observed by the displacement of a bead conjugated with anti-LDL antibody (*open circles*) or with non-activating anti-integrin antibody (K-20) (*closed circles*) in normal solution. $[Ca^{2+}]_i$ increases were induced only when the FN-bead was displaced in the normal solution (*closed triangles*). Symbols except closed *triangles* are overlapped due to the $[Ca^{2+}]_i$ transients are low. (**e**) $[Ca^{2+}]_i$ microdomains 2–4 ms after the onset of the stimulation are shown as *red spots*. These spots are located in the vicinity of integrin clusters (*green*). The *upper left panel* in (**e**) shows approximately 10 $[Ca^{2+}]_i$ microdomains. The *middle left panel* shows integrin and the *lower left panel* shows an overlay of the $[Ca^{2+}]_i$ microdomain and the integrin. The *right-hand panels* in (**e**) show another example of the $[Ca^{2+}]_i$ microdomains 0–2 ms after the onset of the stimulation. Data in panels (**b**)–(**e**) are based on our previous report (Hayakawa et al. 2008)

displacement induced an inward current (23.4 ± 4 pA, $n = 15$) in less than 10 ms, and the current peaked within 100 ms (Fig. 1.4b) then gradually declined. This transient inward current was also significantly reduced by 20 μM Gd^{3+} (91.5 ± 3.1% inhibition, $n = 4$; Fig. 1.4b), suggesting that they are from the same origin – MS channels. The short delay (<10 ms) implies that MS channels were activated directly not via biochemical processes (e.g., second messengers or G-proteins).

1.2.6 Direct Mechanical Stretching of Actin Stress Fibers by Dragging Beads Optically to Activate MS Channels

We developed an innovative technique to test the hypothesis directly that mechanical stress in the actin cytoskeleton activates MS channels. Beads that were coated with the actin cytoskeleton binding agent phalloidin were microinjected to cells through a glass micropipette. The injected beads and actin stress fibers were imaged by confocal microscopy (Fig. 1.5b), showing that most of the beads (or aggregates of beads) and stress fibers were overlapped in the same optical slice. In addition, live imaging of the preparation showed that the beads stayed in the same position, suggesting that the beads were closely associated with stress fibers and/or actin networks that connect stress fibers.

A traction force to actin cytoskeleton was applied by dragging a bead aggregate (approximately 400 nm in diameter) with laser tweezers. MS channel currents were recorded with the whole-cell patch-clamp technique while monitoring the position of the trapping point of laser tweezers (Fig. 1.5a). When the trapping point passed the aggregate, a transient inward current was evoked (Fig. 1.5c) and returned to a basal level in less than 1 s. For a second stimulation, the direction of the movement of the trapping point was reversed and passed the same aggregate, which again evoked an inward current with similar amplitude (Fig. 1.5c, right arrow). The average amplitude of the inward current was 7.4 ± 1.1 pA ($n = 22$), which was 32% of that induced by FN-bead displacement. The amplitude of the force of the laser trapping was estimated at 5.5 pN. When the laser-trapping focus passed an aggregate of phalloidin-conjugated beads, the $[Ca^{2+}]_i$ increased, suggesting that the Ca^{2+}-permeable MS channels are activated by direct mechanical manipulation of actin cytoskeleton. When a nonlabeled bead was trapped and moved by the optical tweezers, force would be transmitted to the substrate in a similar way without activating MS channels; these beads were displaced slightly and were probably stopped by their interaction with subcellular structures, such as microtubules, intermediate filaments or internal membranes. The stress in these structures was not transmitted to the MS channels or perhaps was not large enough to activate them.

The above results, showing that MS channels are activated by the stress in actin stress fibers terminated at basal FCs, leads to the hypothesis that MS channels in HUVECs locate near FCs. To test this idea, we examined the hypothetical colocalization of MS channels and FCs by imaging the $[Ca^{2+}]_i$ microdomain that comprises

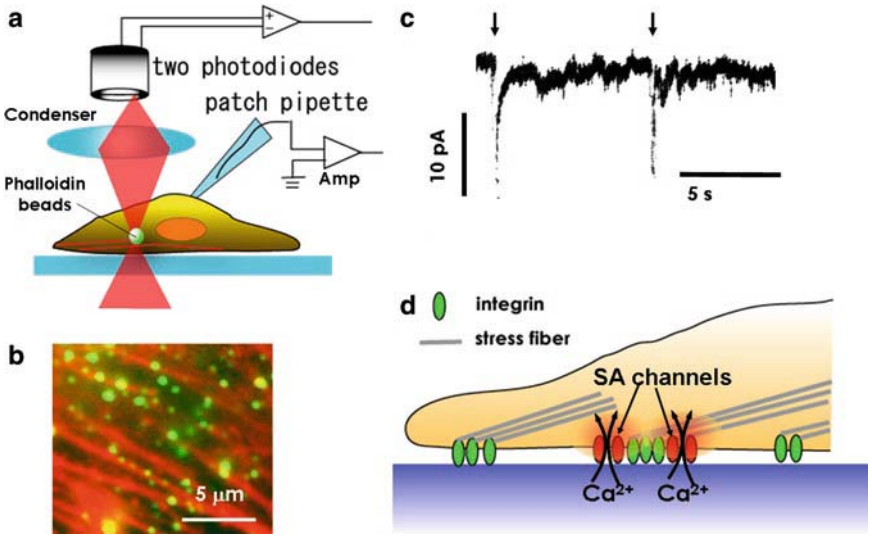

Fig. 1.5 Activation of MS channels by applying mechanical force to beads attached to actin stress fibers. (**a**) Phalloidin-conjugated 40 nm fluorescent beads were microinjected into HUVECs. These beads bound to the actin stress fibers and were trapped by laser optical tweezers. The movement of the trapping point was monitored with two photodiodes. Whole-cell patch-clamp recordings were made from the same cell. (**b**) Phalloidin-conjugated *green* fluorescent beads were located along the actin stress fibers (*red*). The cell was fixed 30 min after microinjection and stained with Rhodamine–phalloidin in this case. (**c**) A transient inward current was induced when the optical tweezers transiently passed an aggregate of phalloidin-coated beads (shown by the *two arrows*). (**d**) A schematic drawing of distribution of integrin clusters (*green*) and MS channels (*red*). The mechanical stress in actin stress fibers activates MS channels in the vicinity of the integrin clusters and induces Ca^{2+} influx to cytosol (*arrows*). This ionic flow is detected by the patch-clamp amplifier illustrated in panel (**a**). The data in panels (**b**) and (**c**) are based on our previous report (Hayakawa et al. 2008)

high-$[Ca^{2+}]_i$ regions at the cytoplasmic vestibule of Ca^{2+}-permeable channels (Zenisek et al. 2003). We imaged $[Ca^{2+}]_i$ microdomains using high-speed evanescent field microscopy, while monitoring the distribution of FCs as described in the following section.

1.2.7 $[Ca^{2+}]_i$ Microdomains in the Vicinity of the FCs Apparently Correspond to the MS Ca^{2+} Permeable Channels

In order to visualize the locus of the $[Ca^{2+}]_i$ microdomains precisely, it is necessary to acquire a fast snapshot (~milliseconds) of the $[Ca^{2+}]_i$ increase immediately after the onset of mechanical stimulation. We imaged the distribution of β1 integrin in living HUVECs, as previously described (Kawakami et al. 2001). In this experiment, $[Ca^{2+}]_i$

transients under the bead were imaged with a single brief (2 ms duration) evanescent laser illumination at, or 2 ms after, the onset of mechanical stimulation (Fig. 1.4e). A mean of 4 ± 0.94 (±SEM; $n = 8$) $[Ca^{2+}]_i$ microdomains appeared in the vicinity of FCs underneath the FN bead with 2 ms of illumination; the diameter of the microdomain was 0.96 ± 0.07 μm ($n = 33$), which agrees with the value in a previous report (Zou et al. 2002) and also with theoretical estimations. A recent study demonstrates that a Ca^{2+} microdomain reflects the activation of a single MS channel (Zou et al. 2002). The diameter of the Ca^{2+} microdomain (2.2 μm, 15 ms after channel opening) is similar to that imaged in this study, supporting the idea that it is possible to image the activation of a single MS channel or a small number of MS channels in the cluster. A theoretical estimation of the size of a Ca^{2+} microdomain also supports the above idea. Using the diffusion constant of Ca^{2+} in cytoplasm (0.6×10^{-6} cm^2/s; Hodgkin and Keynes 1957), the diameter of the Ca^{2+} microdomain 4 ms after the opening of a Ca^{2+} channel is calculated to be 1.1 μm, a value close to 0.96 μm in this study.

The number of $[Ca^{2+}]_i$ microdomains also principally agrees with the number of MS channels estimated from our whole-cell current measurements; the peak amplitude of the whole-cell MS current (23 pA) evoked by displacing a FN bead corresponds to 14–24 MS channels, given that the conductance of a single MS channel in HUVECs ranges from 24 to 40 pS (Lansman et al. 1987; Popp et al. 1992; Yao et al. 2001). If half of them were located on the basal surface of the cell, we would expect to see 7–12 channels (or microdomains) under these recording conditions. This is in the same order of the number in the above observation (approximately 4). All these results support the idea that the $[Ca^{2+}]_i$ microdomain in this study represents a single activated MS channel or a single cluster of a few MS channels. Interestingly, the center of individual $[Ca^{2+}]_i$ microdomains did not overlap with FCs in all $[Ca^{2+}]_i$ microdomains examined, but rather lay ca. 800 nm from the center of FCs (Fig. 1.4e); the area of integrin clusters did not overlap that of $[Ca^{2+}]_i$ microdomains. These results suggest that MS channels in the vicinity of FCs were activated by the force exerted along certain structures, possibly submembranous cytoskeletons, which may link MS channels with the FCs.

The importance of the cytoskeleton for activating MS channels has been repeatedly suggested, based on electrophysiological analyses of single MS channel activities (Sachs 1991; Sokabe et al. 1991; Sukharev et al. 1999; Yao et al. 2001). However, evidence from the studies on cytoskeleton involvement in cell mechanotransduction was indirect. The present study has succeeded in providing direct evidence on this hypothesis by a combination of electrophysiological, advanced imaging and laser trapping techniques.

In HUVECs, the force generated by the laser trapping (5.5 pN) was most likely transmitted through an actin filament to MS channels, where it activated them. The resulting inward current was ~7.4 pA at –40 mV, which corresponded to an activation of 5–8 MS channels. This suggests that a sub-pN force could activate a single MS channel in intact cells. It should be noted that, although there are a large number of channels within a cell, only a very limited number of channels (5–8 in the above case) could be activated by the optical manipulation of actin filaments.

We speculate that these relatively small forces (sub-pN) work on the MS channels of intact HUVECs, compared with activation forces in MscL of *Escherichia coli* (Sukharev et al. 1999; Gullingsrud and Schulten 2003), where approximately 40 pN was used in MD simulations, suggesting that cytoskeletal structures work as an efficient force-transmitting and -focusing structure to confer higher mechanosensitivity on the MS channel in eukaryotic cells. This complex mechanosensing machinery would evolve from simple prokaryotes to complex eukaryotes. The molecular basis of the sensitivity increase in mechanosensing by cytoskeleton channel complex is not yet clarified.

A very small fraction of the force applied to the cell surface was still sufficient to activate MS channels. The force applied to the cell surface by the FN bead (35 nN) induced an inward current of 23 pA, whereas the optical manipulation (5.5 pN) of the actin cytoskeleton induced an inward current of 7.4 pA. These results suggest that most of the force on the FAs (or integrins) would be transmitted to the extracellular substrate via cytoskeleton, organelles and FAs. A very small fraction of the force activates MS channels. The specific molecular components that transmit the force from an actin stress fiber to the MS channels presumably form a structural linkage, but they are not yet identified, remaining an interesting subject for future studies.

1.3 Roles of Mechanosensing in Cell Migration

The studies mentioned above not only provide direct evidence that development of tension in actin stress fibers can activate MS channels in intact cells but also reveal a new function of the actin cytoskeleton as a force-transmitting and -focusing device between integrins and MS channels. Such a concept has already been suggested in previous studies based on indirect observations (Doyle and Lee 2005; Hu et al. 2003; Munevar et al. 2004). Taken together, these studies along with ours open the door to a complex but intriguing world of cellular mechanotransduction involving remote activation and regulation of MS channels, since stress in the actin cytoskeleton changes during a variety of mechano-related cell behaviors, such as morphogenesis and locomotion. A good example can be seen in the locomotion of keratocytes (Doyle and Lee 2005), in which increased traction stresses induce a Gd^{3+}-sensitive $[Ca^{2+}]_i$ transient change, resulting in adhesion disassembly and rapid retraction at the rear of the cell. It is suggested that stress in the actin cytoskeleton will be focused on the MS channel to induce its activation followed by Gd^{3+}-sensitive Ca^{2+} entry.

The relationship between MS channels and cell adhesion has also been discussed in a recent report (Doyle and Lee 2005). A range of cell behaviors, including cell migration (Doyle and Lee 2005; Munevar et al. 2004; Tanaka et al. 2005) and morphogenesis (Naruse et al. 1998b) are inhibited by the potential MS channel blocker Gd^{3+}. Stretching forces applied through flexible substrata also induced increases in both $[Ca^{2+}]_i$ and traction forces in NIH3T3 fibroblasts (Munevar et al. 2004). They suggest that stretch-activated Ca^{2+} entry in the frontal region regulates

the organization of focal adhesions and the output of mechanical forces. The mechanotransduction mechanism proposed in this study, exerted by a molecular complex of MS channel, cytoskeleton, and cell adhesion, evidently plays an important role in these cellular functions.

In nerve growth cones, the role of MS channels in migration has not been totally clarified. TRPC1, a problematic MS channel candidate (Maroto et al. 2005; Gottlieb et al. 2008), may be involved in turning (Wang and Poo 2005).

1.4 Future Perspectives

Cells sense stress in the membrane and/or cytoskeletons. At present, stress is estimated from the strain of materials with known elastic modulus. However, the quantitative estimation of stress in the subcellular structures is generally difficult. In the case of membrane voltage, it is directly measured with microelectrodes or patch-clamp recording techniques; membrane voltage is also estimated with voltage-sensitive dyes. A technique for estimating the stress in the subcellular structures is truly required. FRET (fluorescence resonance energy transfer) is introduced to estimate conformational changes in proteins in response to amphipaths (chemical compounds to induce stress in the membrane or proteins) (Corry et al. 2005; Machiyama et al. 2009). This technique will also be applicable to the detection of stress in the subcellular structures. Development of methods for detecting stress in molecules will promote a new field of science, mechanobiology, which will open a way to explore the mechano-stress-mediated interactions between biomolecules, intracellular signaling, cell remodeling, and cell migration.

Acknowledgments This work was supported in part by Grants-in-aid for General Scientific Research (#13480216 to M.S. and #14580769 to H.T.), Scientific Research on Priority Areas (#15086270 to M.S.) and Creative Research (#16GS0308 to M.S.) from the Ministry of Education Science Sports and Culture and a grant from Japan Space Forum (to M.S. and H.T.).

References

Block SM (1990) Optical tweezers: a new tool for biophysics. In: Noninvasive techniques in cell biology. Wiley-Liss Inc, New York, pp 375–402

Byfield FJ, Aranda-Espinoza H, Romanenko VG, Rothblat GH, Levitan I (2004) Cholesterol depletion increases membrane stiffness of aortic endothelial cells. Biophys J 87:3336–3343

Corey DP, Garcia-Anoveros J, Holt JR, Kwan KY, Lin SY, Vollrath MA, Amalfitano A, Cheung ELM, Derfler BH, Duggan A, Geleoc GSG, Gray PA, Hoffman MP, Rehm HL, Tamasauskas D, Zhang DS (2004) TRPA1 is a candidate for the mechanosensitive transduction channel of vertebrate hair cells. Nature 432:723–730

Corry B, Rigby P, Liu ZW, Martinac B (2005) Conformational changes involved in MscL channel gating measured using FRET spectroscopy. Biophys J 89:L49–L51

Dai J, Sheetz MP (1995) Mechanical properties of neuronal growth cone membranes studied by tether formation with laser optical tweezers. Biophys J 68:988–996

Dai J, Sheetz MP (1999) Membrane tether formation from blebbing cells. Biophys J 77:3363–3370
Dembo M, Wang YL (1999) Stresses at the cell-to-substrate interface during locomotion of fibroblasts. Biophys J 76:2307–2316
Doyle AD, Lee J (2005) Cyclic changes in keratocyte speed and traction stress arise from Ca^{2+}-dependent regulation of cell adhesiveness. J Cell Sci 118:369–379
Drake CJ, Davis LA, Hungerford JE, Little CD (1992) Perturbation of beta 1 integrin-mediated adhesions results in altered somite cell shape and behavior. Dev Biol 149:327–338
Du HP, Gu GQ, William CM, Chalfie M (1996) Extracellular proteins needed for C-elegans mechanosensation. Neuron 16:183–194
Evans EA, Waugh R (1977) Osmotic correction to elastic area compressibility measurements on red-cell membrane. Biophys J 20:307–313
Fukushige T, Siddiqui ZK, Chou M, Culotti JG, Gogonea CB, Siddiqui SS, Hamelin M (1999) MEC-12, an alpha-tubulin required for touch sensitivity in C-elegans. J Cell Sci 112:395–403
Giannone G, Jiang G, Sutton DH, Critchley DR, Sheetz MP (2003) Talin1 is critical for force-dependent reinforcement of initial integrin-cytoskeleton bonds but not tyrosine kinase activation. J Cell Biol 163:409–419
Gottlieb P, Folgering J, Maroto R, Raso A, Wood TG, Kurosky A, Bowman C, Bichet D, Patel A, Sachs F, Martinac B, Hamill OP, Honore E (2008) Revisiting TRPC1 and TRPC6 mechanosensitivity. Pflugers Archiv Eur J Physiol 455:1097–1103
Gullingsrud J, Schulten K (2003) Gating of MscL studied by steered molecular dynamics. Biophys J 85:2087–2099
Hayakawa K, Tatsumi H, Sokabe M (2008) Actin stress fibers transmit and focus force to activate mechanosensitive channels. J Cell Sci 121:496–503
Hirata H, Tatsumi H, Sokabe M (2004) Tension-dependent formation of stress fibers in fibroblasts: a study using semi-intact cells. JSME Int J Ser C 47:962–969
Hodgkin AL, Keynes RD (1957) Movements of labelled calcium in squid giant axons. J Physiol (Lond) 138:253–281
Hu SH, Chen JX, Fabry B, Numaguchi Y, Gouldstone A, Ingber DE, Fredberg JJ, Butler JP, Wang N (2003) Intracellular stress tomography reveals stress focusing and structural anisotropy in cytoskeleton of living cells. Am J Physiol Cell Physiol 285:C1082–C1090
Iba T, Sumpio BE (1991) Morphological response of human endothelial cells subjected to cyclic strain in vitro. Microvasc Res 42:245–254
Imai K, Tatsumi H, Katayama Y (2000) Mechanosensitive chloride channels on the growth cones of cultured rat dorsal root ganglion neurons. Neuroscience 97:347–355
Jacobson BS, Cronin J, Branton D (1978) Coupling polylysine to glass beads for plasma membrane isolation. Biochim Biophys Acta 506:81–96
Kawakami K, Tatsumi H, Sokabe M (2001) Dynamics of integrin clustering at focal contacts of endothelial cells studied by multimode imaging microscopy. J Cell Sci 114:3125–3135
Kojima H, Ishijima A, Yanagida T (1994) Direct measurement of stiffness of single actin filaments with and without tropomyosin by in vitro nanomanipulation. Proc Natl Acad Sci USA 91:12962–12966
Lansman JB, Hallam TJ, Rink TJ (1987) Single stretch-activated ion channels in vascular endothelial cells as mechanotransducers? Nature 325:811–813
Machiyama H, Tatsumi H, Sokabe M (2009) Structural changes in the cytoplasmic domain of the mechanosensitive channel MscS during opening. Biophys J 97:1048–1057
Maroto R, Raso A, Wood TG, Kurosky A, Martinac B, Hamill OP (2005) TRPC1 forms the stretch-activated cation channel in vertebrate cells. Nat Cell Biol 7:179–185
Munevar S, Wang Y, Dembo M (2001) Traction force microscopy of migrating normal and H-ras transformed 3T3 fibroblasts. Biophys J 80:1744–1757
Munevar S, Wang YL, Dembo M (2004) Regulation of mechanical interactions between fibroblasts and the substratum by stretch-activated Ca^{2+} entry. J Cell Sci 117:85–92

Naruse K, Sokabe M (1993) Involvement of stretch-activated ion channels in Ca^{2+} mobilization to mechanical stretch in endothelial cells. Am J Physiol 264 : C1037–C1044

Naruse K, Sai X, Yokoyama N, Sokabe M (1998a) Uni-axial cyclic stretch induces c-src activation and translocation in human endothelial cells via SA channel activation. FEBS Lett 441 : 111–115

Naruse K, Yamada T, Sokabe M (1998b) Involvement of SA channels in orienting response of cultured endothelial cells to cyclic stretch. Am J Physiol 274 : H1532–H1538

Pollard TD, Borisy GG (2003) Cellular motility driven by assembly and disassembly of actin filaments. Cell 112 : 453–465

Popp R, Hoyer J, Meyer J, Galla HJ, Gogelein H (1992) Stretch-activated non-selective cation channels in the antiluminal membrane of porcine cerebral capillaries. J Physiol 454 : 435–449

Pourati J, Maniotis A, Spiegel D, Schaffer JL, Butler JP, Fredberg JJ, Ingber DE, Stamenovic D, Wang N (1998) Is cytoskeletal tension a major determinant of cell deformability in adherent endothelial cells? Am J Physiol 274 : C1283–C1289

Ridley AJ, Schwartz MA, Burridge K, Firtel RA, Ginsberg MH, Borisy G, Parsons JT, Horwitz AR (2003) Cell migration: integrating signals from front to back. Science 302 : 1704–1709

Sachs F (1991) Mechanical transduction by membrane ion channels: a mini review. Mol Cell Biochem 104 : 57–60

Shi F, Chiu YJ, Cho YS, Bullard TA, Sokabe M, Fujiwara K (2007) Down-regulation of ERK but not MEK phosphorylation in cultured endothelial cells by repeated changes in cyclic stretch. Cardiovasc Res 73 : 813–822

Shirinsky VP, Antonov AS, Birukov KG, Sobolevsky AV, Romanov YA, Kabaeva NV, Antonova GN, Smirnov VN (1989) Mechano-chemical control of human endothelium orientation and size. J Cell Biol 109 : 331–339

Sokabe M, Sachs F, Jing Z (1991) Quantitative video microscopy of patch clamped membranes stress, strain, capacitance, and stretch channel activation. Biophys J 59 : 722–728

Sukharev SI, Sigurdson WJ, Kung C, Sachs F (1999) Energetic and spatial parameters for gating of the bacterial large conductance mechanosensitive channel, MscL. J Gen Physiol 113 : 525–540

Szaszak M, Gaborik Z, Turu G, McPherson PS, Clark AJ, Catt KJ, Hunyady L (2002) Role of the proline-rich domain of dynamin-2 and its interactions with Src homology 3 domains during endocytosis of the AT1 angiotensin receptor. J Biol Chem 277 : 21650–21656

Tanaka K, Naruse K, Sokabe M (2005) Effects of mechanical stresses on the migrating behavior of endothelial cells. In: Wada H (ed) Biomechanics at micro and nanoscale levels, vol I. World Scientific Publishing, Singapore, pp 75–87

Tatsumi H, Katayama Y (1999) Growth cones exhibit enhanced cell–cell adhesion after neurotransmitter release. Neuroscience 99 : 855–865

Wang GX, Poo MM (2005) Requirement of TRPC channels in netrin-1-induced chemotropic turning of nerve growth cones. Nature 434 : 898–904

Wang JG, Miyazu M, Matsushita E, Sokabe M, Naruse K (2001) Uniaxial cyclic stretch induces focal adhesion kinase (FAK) tyrosine phosphorylation followed by mitogen-activated protein kinase (MAPK) activation. Biochem Biophys Res Commun 288 : 356–361

Yao X, Kwan H, Huang Y (2001) Stretch-sensitive switching among different channel sublevels of an endothelial cation channel. Biochim Biophys Acta 1511 : 381–390

Zamir E, Katz BZ, Aota S, Yamada KM, Geiger B, Kam Z (1999) Molecular diversity of cell-matrix adhesions. J Cell Sci 112(Pt 11) : 1655–1669

Zenisek D, Davila V, Wan L, Almers W (2003) Imaging calcium entry sites and ribbon structures in two presynaptic cells. J Neurosci 23 : 2538–2548

Zhang Y, Gao F, Popov VL, Wen JW, Hamill OP (2000) Mechanically gated channel activity in cytoskeleton-deficient plasma membrane blebs and vesicles from *Xenopus* oocytes. J Physiol (Lond) 523 : 117–130

Zou H, Lifshitz LM, Tuft RA, Fogarty KE, Singer JJ (2002) Visualization of Ca^{2+} entry through single stretch-activated cation channels. Proc Natl Acad Sci USA 99 : 6404–6409

http://www.springer.com/978-4-431-89756-9

Mechanosensing Biology
Noda, M. (Ed.)
2011, XIII, 219 p., Hardcover
ISBN: 978-4-431-89756-9